Critical dopant concentration in polyacetylene and phase diagram from a continuous four-Fermi model

Heron Caldas,[1,*] Jean-Loïc Kneur,[2,†] Marcus Benghi Pinto,[3,‡] and Rudnei O. Ramos[4,§]
[1]*Departamento de Ciências Naturais, Universidade Federal de São João del Rei, 36300-000 São João del Rei, Minas Gerais, Brazil*
[2]*Laboratoire de Physique Théorique et Astroparticules, CNRS-UMR5207, Université de Montpellier II, F-34094 Montepellier Cedex 5, France*
[3]*Departamento de Física, Universidade Federal de Santa Catarina, 88040-900 Florianópolis, Santa Catarina, Brazil*
[4]*Departamento de Física Teórica, Universidade do Estado do Rio de Janeiro, 20550-013 Rio de Janeiro, Rio de Janeiro, Brazil*
(Received 22 February 2008; revised manuscript received 7 April 2008; published 14 May 2008)

The optimized perturbation theory (OPT) method, at finite temperature and finite chemical potential, is applied to the field theory model for polyacetylene. The critical dopant concentration in *trans*-polyacetylene is evaluated and compared to available experimental data and to previous calculations. The results obtained within the OPT go beyond the standard mean-field (or large-N) approximation by explicitly including finite N effects. A critical analysis of the possible theoretical prescriptions to implement and interpret these corrections to the mean-field results, given the available data, is given. For the typical temperatures probed in the laboratory, our results show that the critical dopant concentration is only weakly affected by thermal effects.

DOI: 10.1103/PhysRevB.77.205109 PACS number(s): 64.60.A−, 71.30.+h, 11.10.Kk

I. INTRODUCTION

About three decades ago, a remarkable discovery was made that *trans*-polyacetylene $(CH)_x$ doped with halogens could behave as a metal, exhibiting electrical conductivity.[1] Since then, several striking features have been shown by conjugated polymers such as electronic, optical, and magnetic properties, which give these materials a wide range of applicability.[2–5] Before reaching the metallic state, polyacetylene can be converted into a semiconductor depending on the concentration of dopant y, which is defined as the number of doped electrons per carbon atom. For the lower dopant concentration, the conduction can be described in terms of topological excitations such as (spinless charged) polarons, bipolarons, or solitons.[6] Experiments have also shown that the observed nonmetal to metal transition in polyacetylene, which typically happens when the dopant concentration is increased to a critical value $y_c \approx 6\%$, corresponds to a first-order transition.[7]

From the theoretical point of view, the role of the (self-localized) solitons in the charge-transport process is successfully described by the Hamiltonian model proposed by Su–Shrieffer–Heeger (SSH).[8] SSH were primarily interested in the low-energy excitations of the one-dimensional polymer. In this case, the electronic correlation length ξ becomes much larger than the lattice constant a, and an effective Hamiltonian model, incorporating only the electron-phonon coupling as an interaction term and neglecting electron-electron Coulomb repulsion was shown to be able to give a very good description of the system. To take electron-electron interactions into account, extended versions of the SSH Hamiltonian, such as Hubbard models,[5,9] have been employed later.

The continuum limit of the SSH Hamiltonian is known as the Takayama–Lin-Liu–Maki (TLM) model,[10] which is a field theory with two-flavor Dirac fermions. The TLM model gives a very good approximation to the discrete SSH model provided that two conditions hold: The band gap (denoted as E_{gap}) between σ electron bonding and antibonding states is much smaller than the π-bandwidth (denoted as W) and the typical distance between the neighboring single-electron levels near the Fermi energy is much smaller than the gap. The first condition is automatically fulfilled for *trans*-polyacetylene, wherein from the typical measured values $E_{\mathrm{gap}}/W \simeq (1.8\ \mathrm{eV})/(10\ \mathrm{eV}) = 0.18$,[6] while the second one is met provided that the application is for a chain with a large size.[11] At the same time, in many conducting polymers, the characteristic correlation length ξ is much larger than the lattice constant a. These two quantities are related to E_{gap} and W by $\xi/a = W/E_{\mathrm{gap}}$.[6]

Some authors[12] have recognized that the corresponding Lagrangian of the TLM model is analogous to a field theoretical model for fermions with quartic self-interactions in 1+1 dimensions, which is also known as the Gross–Neveu (GN) model.[13] It is worth recalling that the large-N, or mean-field approximation (MFA), predicts that at $T=0$, the GN model in 1+1 dimensions suffers a first-order phase transition at the critical chemical potential value $\mu_c = \Delta_0/\sqrt{2}$, where Δ_0 is the order parameter value at $T=0=\mu$.[14] Other works that made use of the GN model applied to the study of the properties of polyacetylene include Refs. 15 and 16. However, to our knowledge, the issue of investigating the phase diagram and temperature effects in the dopant concentration in polyacetylene has not been addressed, within the context of the GN model, so far.

Since we can relate the dopant concentration in terms of the chemical potential, the GN model works as an analog model that can describe, in field theory language, the nonmetal to metal phase transition observed in the *trans*-$(CH)_x$. An early study of the transition from the (chiral symmetry broken) low-density to the (symmetry restored) high-density phase has been performed by Chodos and Minakata[17] by using the GN model by assuming fermions with $N=2$ flavors, but considering only the leading order in a $1/N$ expansion. Despite this approximation, they found an excellent agreement, of about 6%, between the theoretical and experi-

mental critical doping concentration y_c. Later, they used a mixture of the thermodynamic Bethe ansatz (TBA) and the $1/N$ expansion at the next to leading order (NLO) to evaluate finite N corrections to μ_c.[18] Surprisingly, their NLO does not agree so well with the experimental results, deviating by about 20%. One of our main motivations in the present work is to shed some light into this rather peculiar behavior. After all, one expects that finite N corrections should improve convergence, especially in a case wherein $N=2$, such as the case in the theoretical model description of polyacetylene. With this aim, we start by remarking that the critical dopant concentration y_c is related to the critical density ρ_c and the equilibrium space a between the x coordinates of successive CH groups in the undimerized structure by $y_c=\rho_c a$. However, Chodos and Minakata[18] did not compute the finite N corrections to the critical density ρ_c, but rather to the value of the chemical potential μ_c. Nevertheless, they concluded that for $N=2$, $\rho_c(N)$ should change by about 20% since it is proportional to $\mu_c(N)$, which changes by the same amount. We believe that this conclusion is not necessarily right since additional N and/or coupling (λ) dependent factors, $\mathcal{H}(\lambda,N)$, could appear when obtaining ρ by deriving the pressure with respect to μ, so that $\rho_c(N)$ could be proportional to $\mathcal{H}(\lambda,N)\mu_c(N)$, where, for example, $\mathcal{H}(\lambda,N\to\infty)\to 1$ in the mean-field approximation. Second, ρ depends on parameter values such as E_{gap} and W that set $\xi/a=W/E_{\mathrm{gap}}$, but only the value $\xi/a\simeq 7$, which corresponds to the original SSH parameters[8] $E_{\mathrm{gap}}=1.4\mathrm{eV}$ and $W=10\mathrm{eV}$, was considered in Refs. 17 and 18. We must recall that the original SSH parameter values, especially the one regarding E_{gap}, have already been further updated in the Ref. 6.

Here, we shall again investigate the same problem considering the $1+1$ dimensional GN model but not restricting the analysis to the large-N approximation. On general grounds, one may eventually wonder on the relevance of going beyond the large N (or equivalently mean-field) approximation in the present context, given that the equivalence between the original TLM model and the GN field theory was established, strictly speaking, at the mean-field level: Indeed, there are important phenomenological aspects and properties of the polyacetylene that are anyway not correctly described by the sole TLM (for a review on both the successes and the limitations of the TLM/GN equivalence, see, e.g., Ref. 19). Nevertheless, it appears sensible here to further push the correspondence in this direction at least because the TLM model is effectively a two-flavor only model: Since there are some results and techniques go beyond large N are available, these can be expected to improve the comparison of the GN model to polyacetylene data, as we shall see later. In this work, we use the method of the optimized perturbation theory (OPT),[20] which is a nonperturbative method allowing one to consider corrections going beyond the large-N (or mean-field) approximation. Our aim is to obtain relations for ρ_c which include finite N corrections. For this, we will reconsider Landau's free energy density for the $1+1$ dimensional GN model that was recently derived by some of the present authors in Ref. 21, wherein the OPT results for the phase diagram show how this method correctly improves over mean-field results, in accordance with Landau's theorem for phase transitions in one space dimensions. In the same reference, one finds analytical equations for the order parameter and chemical potential with dependence on N, which turn out to be crucial for the present application. A detailed description of how the method works can be found in Ref. 21 and references therein.

In the present application, we will indeed show that within the OPT, one can obtain the critical dopant concentration y_c in a consistent way, which produces results that are in very good agreement with the experimental values for the *trans*-$(\mathrm{CH})_x$ when up-to-date parameter values are considered. For completeness, however, we will examine several possible theoretical prescriptions to implement and interpret these corrections to the mean-field results. More precisely, as we shall see, the corrections to the mean field may be interpreted in different ways within the context of polyacetylene. This is due to the fact that its description in terms of the Gross–Neveu field theory model is, strictly speaking, only an approximation. We shall also pay attention to the nonnegligible experimental error on some of the relevant available data. Apart from considering finite N corrections to y_c, we also estimate how thermal effects affect this quantity.

It is worth mentioning that an extension to the $2+1$ dimensional GN theory is straightforward and may be of use in the investigation of superconducting electrons in quasi-two-dimensional systems.[22] In connection with the $2+1$ dimensional GN model, the OPT allows[23] the redrawing of its phase diagram, leading to the precise location of a tricritical point in the $T-\mu$ plane and the discovery of a mixed "liquid-gas" phase that remained undetermined for almost twenty years, since the first mean-field results appeared.[24] The compatibility of the OPT and Landau's expansion for the free energy density is shown in Ref. 25. In the condensed matter domain, higher order OPT results have considerably improved early applications of the same method,[26] producing some of the most precise analytical values for the shift of the critical temperature ΔT_c of an interacting homogeneous Bose gas when compared to the ideal gas.[27] Finally, the OPT convergence has also been proved in connection with critical theories of Kneur *et al.*[28] and Braaten and Radescu.[29]

As far as thermal effects in the GN model at one space dimension and the application of these results to polyacetylene are concerned, a few comments are appropriate here. We recall that due to a well known no-go theorem,[30–32] for a one-dimensional system at any finite temperature, we should expect no phase transition related to a discrete symmetry breaking (in this case, a discrete chiral symmetry in the massless GN model was considered). This is due to kinklike inhomogeneous configurations[33] that come to dominate the action functional instead of being just homogeneous, constant field configurations. This is to be contrasted to the phase transition observed since long ago in the GN model in one space dimension in the mean-field, large-N approximation.[14] This result is explained by the way the thermodynamic and the mean-field approximation are performed. If the thermodynamic limit is taken before the mean-field approximation, those large nonhomogeneous fluctuations dominate and the theorem is observed. However, if the mean-field approximation is considered first, the fluctuations are suppressed, thus seeming to evade the no-go theorem. Since we are here applying the GN model as an

effective analog model for the polyacetylene and this is in practice a finite size system, we do not expect the theorem to be completely observed here. In fact, a phase transition at finite temperatures is indeed observed and measured in the laboratory. Nevertheless, polyacetylene is a well-known system exhibiting a rich spectrum of nontrivial fluctuations from solitons to polaron excitations.[6] Therefore, we may expect not only homogeneouslike configurations (such as in the mean-field approach) but also that the inclusion of these excitations in any theoretical calculation in this model should be considered. In this context, for example, in the GN field theory model, by accounting for kinklike configurations in the large-N approximation, Thies and co-workers[34] found evidence for a crystal phase that shows up in the extreme $T\sim 0$ and large μ part of the phase diagram, while the other extreme of the phase diagram, for large T and $\mu\sim 0$, seemed to remain identical to the usual large-N results for the critical temperature and tricritical points, which are well known results[14] for the GN model. In this work, we will consider only homogeneous vacuum backgrounds only in our thermodynamical calculations applied to the polyacetylene. By comparing our results to the experimental ones, we can roughly estimate the importance of solitonlike excitations in the system. From our results, we estimate that these effects are expected to be small in the context of applying the GN model as an effective analog model to describe the thermodynamics of polyacetylene at low (laboratory) temperatures.

This work is organized as follows: In Sec. II, we briefly present the TLM model and its relation to a four-fermion theory, which can be identified as the GN model. In Sec. III, we review the computation of the free energy for the GN model by using the OPT method. In the same section, the temperature dependent density is obtained. The gap equation is used to set up the parameter values in Sec. IV. In Sec. V, we show our phase diagrams for the *trans*-polyacetylene $(CH)_x$ both in the $T-\mu$ and $T-\rho$ planes. The critical dopant density, at zero and finite temperatures, is considered in Sec. VI. Our concluding remarks are given in Sec. VII.

II. TAKAYAMA–LIN-LIU–MAKI AND GROSS-NEVEU MODELS

The Takayama–Lin-Liu–Maki (TLM) Hamiltonian is the continuum version for the original SSH model and it is given in terms of a fermionic field ψ and a scalar field Δ representing the coupling of the electron gas to the local value of the dimerization and it is expressed by the Hamiltonian[10]

$$H_{\mathrm{TLM}} = \frac{1}{2\pi\hbar v_F \lambda_{\mathrm{TLM}}}\int dx\Delta^2(x) + \sum_s \int dx\psi^\dagger(x)[-i\hbar v_F\sigma_3\partial_x + \sigma_1\Delta(x)]\psi(x), \tag{2.1}$$

where the sum is over the spin states, σ_i are the Pauli matrices, $v_F=\hbar k_F/m$ is the Fermi velocity, and λ_{TLM} is a dimensionless coupling defined by

$$\lambda_{\mathrm{TLM}} = \frac{2\alpha^2}{\pi t_0 K}, \tag{2.2}$$

where α is the π-electron-phonon coupling constant of the original SSH Hamiltonian, K is the elastic chain deformation constant, and t_0 is the hopping parameter, which is expressed in terms of the Fermi velocity and the equilibrium space a between the x coordinates of successive CH groups in the undimerized structure as $t_0=\hbar v_F/(2a)$.

Note from Eq. (2.1) that a nonvanishing (constant) value for Δ leads to a mass term for the fermions, thus breaking the chiral symmetry exhibited by H_{TLM} and opening an electronic energy gap in the system. The presence of a gap prevents electrons from moving to the conduction band and, thus, the system effectively behaves as a nonmetal. The effect of the addition of dopants to the system is to decrease the electronic energy gap until it vanishes at some critical dopant concentration and the system starts to behave as a metal. In general, a kinetic term for the scalar field emerges when taking the continuum limit of the SSH model. However, we consider the usual adiabatic approximation of neglecting the lattice vibrations, which is valid for energies for the optical-phonons (given by $\hbar\omega_0$) smaller than the gap magnitude (2Δ). In particular, for typical values found for polyacetylene[6] such as $2\Delta\approx 1.8$ eV and $\hbar\omega_0\approx 0.12$ eV, this is regarded as a valid approximation.

The model described by Eq. (2.1) can easily be shown to correspond to a four-Fermi model if we eliminate the scalar field Δ from Eq. (2.1), e.g., by using its equation of motion. Then, putting the TLM model in the Lagrangian density form, one obtains

$$\mathcal{L}_{\mathrm{TLM}} = -\frac{1}{2\pi\hbar v_F\lambda_{\mathrm{TLM}}}\Delta^2 + \psi^\dagger(i\hbar\partial_t - i\hbar v_F\gamma_5\partial_x - \gamma_0\Delta)\psi, \tag{2.3}$$

where we have identified $\gamma_5=-\sigma_3$ and $\gamma_0=\sigma_1$. Now, eliminating Δ from Eq. (2.3) upon using $\gamma_1=i\sigma_2$, as well as the usual relations between the Dirac matrices, leads to

$$\mathcal{L}_{\mathrm{TLM}} = \bar{\psi}(i\hbar\gamma_0\partial_t - i\hbar v_F\gamma_1\partial_x)\psi + \frac{\lambda_{\mathrm{GN}}}{2N}\hbar v_F(\bar{\psi}\psi)^2, \tag{2.4}$$

which is just a four-Fermi Lagrangian density corresponding to the massless GN model[13] where N is the number of fermion flavors ($N=2$ for polyacetylene). In Eq. (2.4), we have used Eq. (2.2) to define the GN coupling as

$$\lambda_{\mathrm{GN}} = N\pi\lambda_{\mathrm{TLM}} = \frac{2N\alpha^2}{t_0 K}. \tag{2.5}$$

III. GROSS–NEVEU MODEL IN THE OPTIMIZED PERTURBATION THEORY

Let us now turn our attention to the implementation of the OPT procedure[20] (for a long but far from complete list of references, please also see Ref. 21 and references therein) within the Lagrangian model density given by Eq. (2.4). Applying the usual OPT interpolation prescription to the *origi-*

nal four-Fermi theory, Eq. (2.4), we define the interpolated theory as

$$\mathcal{L}_\delta(\psi,\bar{\psi}) = \bar{\psi}(i\hbar\gamma_0\partial_t - i\hbar v_F\gamma_1\partial_x)\psi - \eta(1-\delta)\bar{\psi}\psi + \delta\frac{\lambda_{\mathrm{GN}}}{2N}\hbar v_F(\bar{\psi}\psi)^2, \quad (3.1)$$

where η is an arbitrary mass parameter. It is easy to verify that at $\delta=0$, we have a theory of free fermions and the original theory is recovered for $\delta=1$. Now, by reintroducing the scalar field Δ, which can be achieved by adding the quadratic term (corresponding to a Hubbard–Stratonovich transformation)

$$-\frac{\delta N}{2\hbar v_F\lambda_{\mathrm{GN}}}\left(\Delta + \frac{\lambda_{\mathrm{GN}}}{N}\hbar v_F\bar{\psi}\psi\right)^2, \quad (3.2)$$

to $\mathcal{L}_\delta(\psi,\bar{\psi})$, one obtains the interpolated model corresponding to the original TLM model given by Eq. (2.3),

$$\mathcal{L}_\delta = \bar{\psi}(i\hbar\gamma_0\partial_t - i\hbar v_F\gamma_1\partial_x)\psi - \delta\Delta\bar{\psi}\psi - \eta(1-\delta)\bar{\psi}\psi - \frac{\delta N}{2\hbar v_F\lambda_{\mathrm{GN}}}\Delta^2. \quad (3.3)$$

Since Eq. (3.3) is the same model that was already studied in Ref. 21, we do not repeat all the details related to the free energy density derivation here and only the main steps and results relevant for our application to the polyacetylene will be presented.

Generally, the OPT method can be implemented as follows: Any physical quantity $\Phi^{(k)}$ is *perturbatively* computed from the interpolated model, up to some finite order-k in δ, which is formally used only as a bookkeeping parameter and set to unity at the end of the calculation. However, in this process, any (perturbative) result at order k in the OPT remains η dependent. This arbitrary (*a priori*) parameter is then fixed by a variational method that then generates nonperturbative results in the sense that it resums a certain class of perturbative contributions to all orders through self-consistent equations. Such an optimization method is known as the principle of minimal sensitivity (PMS) and amounts to require that $\Phi^{(k)}$ be evaluated at the point where it is less sensitive to this parameter. This criterion translates into the variational relation[35]

$$\left.\frac{d\Phi^{(k)}}{d\eta}\right|_{\delta=1,\eta=\bar{\eta}} = 0. \quad (3.4)$$

The optimum value $\bar{\eta}$ that satisfies Eq. (3.4) must be a function of the original parameters, which includes the couplings, thus generating "nonperturbative" results. In our case, we are interested in evaluating the optimized free energy at finite temperature and density for the scalar field Δ once the fermions have been integrated out.

A. Optimized free energy density

To order- δ, Landau's free energy density (or effective potential, in the language of quantum field theories) was evaluated in Ref. 21 by using functional and diagrammatic techniques. The result is

$$\mathcal{F}(\Delta_c,\eta,T,\mu) = \delta\frac{N\Delta_c^2}{2\lambda_{\mathrm{GN}}v_F\hbar} - \frac{N}{2\pi v_F\hbar}\left\{\eta^2\left[\frac{1}{2}+\ln\left(\frac{M}{\eta}\right)\right] + 2(kT)^2 I_1(\eta,\mu,T)\right\} + \delta\frac{N\eta(\eta-\Delta_c)}{\pi v_F\hbar}\left[\ln\left(\frac{M}{\eta}\right) - I_2(\eta,\mu,T)\right] + \delta\frac{\lambda_{\mathrm{GN}}}{4\pi^2 v_F\hbar}\left\{\eta^2\left[\ln\left(\frac{M}{\eta}\right) - I_2(\eta,\mu,T)\right]^2 + (kT)^2 I_3^2(\eta,\mu,T)\right\}, \quad (3.5)$$

where k is the Boltzmann constant and the functions I_1, I_2, and I_3 are given, respectively, by

$$I_1(\eta,\mu,T) = \int_0^\infty dx\{\ln[1+e^{-\sqrt{x^2+\eta^2/(kT)^2}-\mu/(kT)}] + \ln[1+e^{-\sqrt{x^2+\eta^2/(kT)^2}+\mu/(kT)}]\}, \quad (3.6)$$

$$I_2(\eta,\mu,T) = \int_0^\infty \frac{dx}{\sqrt{x^2+\eta^2/(kT)^2}}\left[\frac{1}{e^{\sqrt{x^2+\eta^2/(kT)^2}+\mu/(kT)}+1} + \frac{1}{e^{\sqrt{x^2+\eta^2/(kT)^2}-\mu/(kT)}+1}\right], \quad (3.7)$$

and

$$I_3(\eta,\mu,T) = \sinh\left(\frac{\mu}{kT}\right)\times\int_0^\infty dx\frac{1}{\cosh(\sqrt{x^2+\eta^2/(kT)^2})+\cosh[\mu/(kT)]}. \quad (3.8)$$

In Eq. (3.5), Δ_c is a constant field configuration for the scalar field and M is an arbitrary energy scale introduced during the regularization process used to compute the appropriate momentum integrals. In the computation performed in Ref. 21, the free energy density has been renormalized by using the $\overline{\mathrm{MS}}$ scheme for dimensional regularization. We also note that Eq. (3.5), which is evaluated at first order in the OPT, already takes into account corrections beyond the large-N result.

By optimizing Eq. (3.5) through the PMS condition, Eq. (3.4), we obtain the optimum value $\bar{\eta}$ for the mass parameter, which is then reinserted back into Eq. (3.5), allowing us to compute the order parameter $\bar{\Delta}_c$ that minimizes the free energy. By using the PMS procedure, we then obtain, from Eq. (3.5), the general factorized result[21]

$$\left\{\left[\mathcal{Y}(\eta,\mu,T)+\eta\frac{d}{d\eta}\mathcal{Y}(\eta,\mu,T)\right]\left[\eta-\Delta_c+\eta\frac{\lambda_{\mathrm{GN}}}{2\pi N}\mathcal{Y}(\eta,\mu,T)\right]+\frac{(kT)^2\lambda_{\mathrm{GN}}}{2\pi N}I_3(\eta,\mu,T)\frac{d}{d\eta}I_3(\eta,\mu,T)\right\}\Bigg|_{\eta=\bar{\eta}}=0, \tag{3.9}$$

where we have defined the function

$$\mathcal{Y}(\eta,\mu,T)=\ln\left(\frac{M}{\eta}\right)-I_2(\eta,\mu,T). \tag{3.10}$$

Considering the λ_{GN}/N dependent solution, one notices that when $N\to\infty$ in Eq. (3.9), $\bar{\eta}=\Delta_c$ and the mean-field standard result is exactly reproduced as usual.[21,36] For finite N, which is our interest here, $\bar{\eta}$ and Δ_c have to be self-consistently found by solving the gap equation $d\mathcal{F}/d\Delta_c=0$ and the PMS equation $d\mathcal{F}/d\eta=0$.[21]

B. Density at finite temperature

The thermodynamical potential (per volume) is defined as the free energy density at its minimum $\Omega(T,\mu)=\mathcal{F}(\bar{\eta},\bar{\Delta}_c,T,\mu)$ and the pressure follows as $P(T,\mu)=-\Omega(T,\mu)$. The density is then obtained by the usual relation $\rho=dP/d\mu$. We must also recall that $d\mathcal{F}/d\Delta_c=0$ at $\Delta_c=\bar{\Delta}_c$ due to the gap equation, and that $d\mathcal{F}/d\eta=0$ at $\eta=\bar{\eta}$ due to the PMS equation. Then, terms such as $(d\mathcal{F}/d\Delta_c)(d\Delta_c/d\mu)$ and $(d\mathcal{F}/d\eta)(d\eta/d\mu)$ do not contribute. One then obtains

$$\rho(T,\mu)=\frac{1}{v_F\hbar}\left[(kT)^2\frac{N}{\pi}I_1'(\eta,\mu,T)+\eta(\eta-\Delta_c)\frac{N}{\pi}I_2'(\eta,\mu,T)-\frac{\lambda_{\mathrm{GN}}}{2\pi^2}\eta^2 I_2(\eta,\mu,T)I_2'(\eta,\mu,T)-\frac{\lambda_{\mathrm{GN}}}{2\pi^2}(kT)^2 I_3(\eta,\mu,T)I_3'(\eta,\mu,T)\right]\Bigg|_{\eta=\bar{\eta},\Delta_c=\bar{\Delta}_c}, \tag{3.11}$$

where the primes indicate derivatives with respect to μ. This result will be considered later when we investigate thermal effects in y_c.

IV. GAP ENERGY AND PARAMETER SET AT $T=0$ AND $\mu=0$

In order to perform a numerical analysis, we must fix all parameters. This can be done by considering the gap energy. In the GN language, the order parameter $\bar{\Delta}_c$ is just the TLM gap parameter which, at $T=0$ and $\mu=0$, we denote as Δ_0. At order-δ, this quantity is given by[21]

$$\Delta_0=M\exp\left\{-\frac{\pi}{\lambda_{\mathrm{GN}}\left(1-\frac{1}{2N}\right)}\right\}\left(1-\frac{1}{2N}\right)^{-1}, \tag{4.1}$$

where M is an arbitrary (at the moment) renormalization scale to be discussed further below. Equation (4.1) explicitly includes corrections beyond large-N, as obtained from our OPT approach. More precisely, by taking the mean-field approximation, $N\to\infty$ in Eq. (4.1), and using the relation $\lambda_{\mathrm{GN}}=N\pi\lambda_{\mathrm{TLM}}$, the OPT result exactly recovers the mean-field result for $N=2$,[6]

$$\Delta_{MF}=M\exp[-1/(2\lambda_{\mathrm{TLM}})], \tag{4.2}$$

as one expects.[21,36]

Now, some remarks concerning the arbitrary energy scale M, and more generally, on the interpretation of Eq. (4.1) in the present polyacetylene context are useful. Usually, in a renormalizable quantum field theory, one can choose arbitrary values for M and λ_{GN} will appropriately run with the scale at a given perturbative order, so that Δ_0 remains scale invariant as dictated by the renormalization group. For the above gap equation, this means that

$$\frac{1}{\lambda_{\mathrm{GN}}(M)}=\frac{1}{\lambda_{\mathrm{GN}}(M_0)}+\frac{\left(1-\frac{1}{2N}\right)}{\pi}\ln\left(\frac{M}{M_0}\right), \tag{4.3}$$

where M_0 is some reference (input) scale. [Note that the N dependence of the running coupling as dictated by Eq. (4.3) differs from the standard RG one, which (at one-loop order) has a coefficient given by $1-1/N$ instead of $1-1/(2N)$. This difference is a result of OPT, which modifies standard one-loop order results in a way expected to improve the latter.] Equation (4.1) or (4.3) indicates that $\lambda(M)$, or equivalently Δ_0, is the only parameter to be fixed. These equations also show that $\lambda(M)\to 0$ as $\ln^{-1}(M/M_0)$ when $M\to\infty$, which is nothing else than the asymptotic freedom displayed by the GN model. However, in the polymer physics case, the interpretation is somewhat different mainly because *both* Δ_0 and the coupling λ_{GN} are measurable quantities, as we shall exploit below. Moreover, in contrast to the renormalizable field theory case, all quantities here are expected to be directly finite, i.e., without the need of renormalization due to the explicit high energy cutoff Λ provided by the π-bandwidth, i.e., $\Lambda\sim W$. While in our calculation we have used dimensional regularization and renormalization mainly for convenience, Eq. (4.1) should be interpreted as giving the *finite*, N-dependent corrections to the large-N results, with the arbitrary scale M (originating from dimensional regularization) to be traded for an explicit cutoff: $M\equiv\Lambda$ of order $\Lambda\sim W$. Now, since M is a parameter from the theory, its precise value is thus a matter of choice to some extent, as it does not need to exactly coincide with the experimental parameter W. This implies, in particular, that the scale M can be dealt with in alternative ways as we shall discuss next.

Consequently, we can consider different possible prescriptions for the basic parameters of the problem given also that some data appear to have non-negligible experimental uncertainties.

(i) First, in the prescription, we label (I), $\lambda_{\mathrm{GN}}(M)$ can be simply set to its phenomenological value given by

TABLE I. The OPT and MFA values for λ_{GN} and M obtained, from the gap equation, for parameter sets A ($2\Delta_0=1.4$eV) and B ($2\Delta_0=1.8$eV), by using prescriptions I–III for fixing the relevant parameters of the model. The common values for both cases are $K=21\text{eV}/\text{Å}^2$, $\alpha=4.1\text{eV}/\text{Å}$, and $W\equiv 4t_0=10$eV.

	I.A	I.B	II.A	II.B	III.A	III.B
λ_{GN}^{OPT}	1.28	1.28	1.42	1.55	1.89	2.07
λ_{GN}^{MFA}	1.28	1.28	1.18	1.30	1.18	1.30
M^{OPT}(eV)	13.85	17.80	10	10	7.5	7.5
M^{MFA}(eV)	8.15	10.47	10	10	10	10

$$\lambda_{GN}(M)=\frac{8N\alpha^2}{WK}, \tag{4.4}$$

where we have used the relation $4t_0=W$. As discussed above, this implicitly defines a scale M once assuming the theoretical prediction of Eq. (4.1).

Regarding the data numerical values, we note that this has been debated for long and different set of values appeared in literature (see, e.g., Refs. 6 and 8). As far as we are aware, it appears,[19] however, that the present widely accepted data values are $K=21\text{eV}/\text{Å}^2$, $\alpha=4.1\text{eV}/\text{Å}$, $2\Delta_0=1.4-1.8$eV, and $W\equiv 4t_0=10$eV, which are essentially the conventional SSH values[8] except for possible higher values of Δ_0,[6] which appears as the less accurately determined experimental input. Consequently, in our study, we shall take this set of input but taking the two extreme values of Δ_0, which we will call sets A and B, respectively, for $2\Delta_0=1.4$ (1.8) eV.

Thus, comparing sets A and B appears to us as a very conservative way of taking those experimental uncertainties into account, although the higher value of $2\Delta_0\sim 1.8$ eV appears to be much more favored in the recent literature. Since all relevant physical quantities (such as the critical density) will depend on the cutoff scale M as already mentioned, one possible prescription is to use Eq. (4.1) to fix the cutoff M value for given $\lambda_{GN}(M)=8N\alpha^2/(WK)$ and Δ_0 within accuracy, i.e., for each of the data sets A and B. Equation (4.1) shows that due to the presence of N dependent constant term $1-1/(2N)$, the OPT and the MFA will predict in this way different M values even when using the same set of input data parameters.

(ii) Another possible prescription, which we dub (II), is to set $M=W$ exactly, which cuts off the spectrum at an energy scale of $-W/2$.[6,19] In such case, $\lambda_{GN}(M=W)$ does not exactly match the experimental value as predicted by Eq. (4.3). Most previous authors appear to have chosen this prescription, i.e., changing the coupling λ_{GN} value in order that the mean-field model best fits the polyacetylene data. We are, however, equally motivated to use the first interpretation since, as already mentioned, the polyacetylene data provide us with a rather precise λ_{GN} value, while there is some intrinsic arbitrariness in the precise cutoff scale value (equivalently in this case, Δ_0 fixes the energy cutoff scale M within some accuracy). [Note also that Eq. (4.3) also allows for any other intermediate prescriptions in which $M\neq W$ and $\lambda_{GN}(M)\neq 8N\alpha^2/(WK)$, but the simultaneous equalities for these quantities is excluded because of the $2\Delta_0=1.4-1.8$eV values.] Actually, the two prescriptions are not fundamentally different: In the first, one uses the arbitrariness of the cutoff to fit the data Δ_0 and λ_{GN}, while in the second, one forces the coupling to fit the two scales Δ_0 and W, but this is essentially translating the arbitrariness of the scale inside the exponential of Eq. (4.1).

(iii) Finally, let us consider yet another possible prescription (or rather interpretation) of the GN model/polyacetylene data connection. It will be defined as prescription (III). Namely, bearing in mind that the equivalence between the original TLM and continuous GN model was strictly established only at the mean-field theory level, we may redefine our OPT corrections in the framework of an *effective* mean-field (EMF) GN description: More precisely, the OPT-modified gap energy Eq. (4.1) can be fitted by the corresponding mean-field expression Eq. (4.2), provided that one redefines "effective" mean-field coupling [note that the meaning of effective coupling here is purely phenomenological, as obtained from a fit, and thus unrelated to the usual effective coupling $\lambda_{GN}(M)$ as above discussed having the RG behavior] λ_{EMF}^* and cutoff W_{EMF}^* as

$$\lambda_{EMF}^*\equiv\lambda_{GN}\left(1-\frac{1}{2N}\right),\quad W_{EMF}^*\equiv M\left(1-\frac{1}{2N}\right)^{-1}, \tag{4.5}$$

together with the identification of these effective parameters to the measured data.

This freedom of prescriptions, as discriminated above as prescriptions I, II, and III, actually reflects that neither the MFA nor the OPT-improved expression of the gap energy is expected to be exact results. If available, an exact, truly nonperturbative calculation of the gap energy would be expected to nicely fit the three independent experimental measurements t_0 (equivalently W), Δ_0, and λ_{GN} (of course, up to limited experimental accuracy). Therefore, for completeness and comparison purposes, in the numerical results we will consider all these prescriptions together with data sets A and B. A summary of the different M and λ_{GN} values for each prescription and data set is given in Table I.

Inspection of Table I, indeed, indicates rather different values of the "bare" coupling λ_{GN} for the three prescriptions, which is essentially due to the large uncertainty in Δ_0 between sets A and B. One should not conclude from this that our description lacks prediction. In fact, as we shall see later, the predictions of our main result on the critical dopant estimate are not strongly dependent on the coupling values and will be only slightly different for the three cases (provided

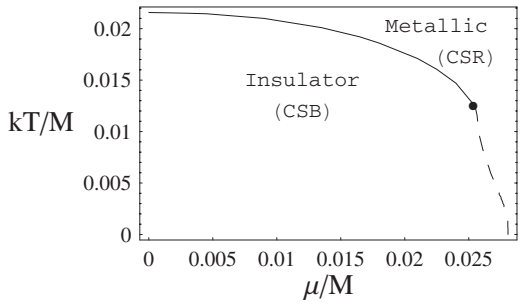

FIG. 1. The OPT phase diagram, in the kT/M-μ/M plane, for $N=2$ and $\lambda=1.28$ (prescriptions IA and IB in Table I). The continuous line represents the second order transition, whereas the dashed line represents the first order transition, and the dot indicates the tricritical point, which occurs at $kT/M \simeq 0.012$ and $\mu/M \simeq 0.025$.

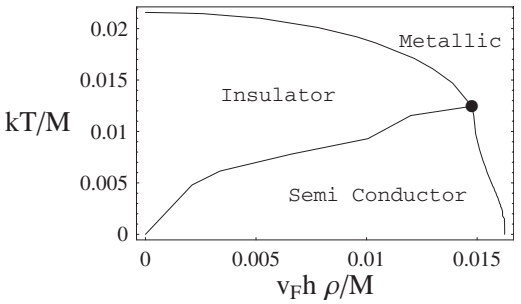

FIG. 2. The OPT phase diagram in the $kT/M-v_F\hbar\rho/M$ plane for $N=2$ and $\lambda=1.28$ (prescriptions IA and IB in Table I). The insulator region is associated with the unsymmetric (dimerized) phase, while the metallic region is associated with the symmetric (undimerized) phase.

that one uses the same experimental data input). Again, the most important variation will be due to the large uncertainty on Δ_0.

V. PHASE DIAGRAMS

Having set the parameters for different prescriptions, we can investigate the phase diagrams for the theory. Let us start by locating the second order and first order transition lines in the $T-\mu$ plane. This is shown in Fig. 1 for the choice of prescription IB. It shows the appearance of a tricritical point around $kT/M \simeq 0.012$ and $\mu/M \simeq 0.025$. Those numbers would slightly change for the other prescriptions, with the overall behavior qualitatively very similar. Although the appearance of a tricritical point is an interesting issue when considering the GN as a toy model for QCD, it has no practical implications for the polyacetylene, in which case one is concerned with temperatures lower than about $T_d \sim 400$K, above which the polyacetylene is unstable and decomposes when heated (instead of melting),[37] that is, $kT_d/M \approx 0.0020$ for $M \approx 17.80$ eV (prescription IB). This type of phase diagram was extensively studied in Ref. 21, wherein analytical expressions for T_c and μ_c as well as useful relations among tricritical point relations can be found.

As emphasized in Sec. I, one of our goals here regards the evaluation of the critical concentration y_c as a function of the temperature. With that aim, one benefits from analyzing the phase diagram in the $T-\rho$ plane since $y_c(T)$ is directly proportional to $\rho_c(T)$. This is shown in Fig. 2. The dot in Fig. 2 indicates the tricritical point above which the transition is of the second kind. The mixed (semiconductor) region is associated to the first order phase transition. At $T=0$, the critical dopant density is approximately $\rho_c(0) \simeq 0.016\text{M}/(v_F\hbar)$. Figure 2 shows the situation wherein the first order transition line, which appears in the $T-\mu$ plane, splits into two lines limiting a coexistence, mixed (semiconducting) region. We note that there are indeed experimental indications of a mixed phase for polyacetylene for concentrations below the critical one.[38] It is also interesting to note, from Fig. 2, that when one evaluates y_c at $T=0$ by using the GN model,[17,18] the only observed transition is from the semiconducting phase to the metallic one. However, even at room temperature (roughly $kT/M \approx 0.0015$), Fig. 2 displays another transition from the (unsymmetric) insulator phase to the (mixed) semiconductor phase that happens at a rather very small density, which is of the order $v_F\hbar\rho/M \sim 10^{-5}$. For this transition, the critical density increases with the temperature. On the other hand, the critical density when going from the (mixed) semiconducting phase to the (symmetric) metallic one seems to slightly decrease for low values of T. Figure 2 also shows that above $\rho_c(0)$, which is computed in the next section, the material is a conductor at any temperature, provided that this temperature is smaller than the degradation temperature T_d. In Sec. VI, we shall devote special attention to this issue since the literature does not seem to indicate any previous studies of the influence of thermal effects in y_c within the models considered here.

VI. CRITICAL DOPANT DENSITY

In this section, we evaluate the critical dopant concentration y_c which, with periodic boundary conditions in the polyacetylene chain, is given simply as $y_c=a\rho_c$. In Sec. VI A, we consider the case $T=0$ by performing a numerical comparison between the MFA and the OPT and using the different sets of parameters presented earlier. Next, we will consider how the temperature affects y_c.

A. Zero temperature case

In this section, we will evaluate the dopant critical density in polyacetylene within the OPT approach, neglecting eventual temperature effects, which will be considered in Sec. VI B. Let us start by taking the limit $T \to 0$ in the free energy density, Eq. (3.5). The various functions defined by Eqs. (3.6)–(3.8), in the $T \to 0$ limit, become

$$\lim_{T\to 0}(kT)^2 I_1(\eta,\mu,T) = -\frac{1}{2}\theta(\mu-\eta)\left[\eta^2 \ln\left(\frac{\mu+\sqrt{\mu^2-\eta^2}}{\eta}\right) - \mu\sqrt{\mu^2-\eta^2}\right], \tag{6.1}$$

$$\lim_{x\to 0} I_2(\eta,\mu,T) = \theta(\mu-\eta)\ln\left(\frac{\mu+\sqrt{\mu^2-\eta^2}}{\eta}\right), \tag{6.2}$$

TABLE II. The critical dopant concentration y_c obtained with the OPT and the MFA obtained from each of the three different prescriptions and two data sets at $T=0$. For reference, we also show the relevant values of ξ/a in each case.

	I.A	I.B	II.A	II.B	III.A	III.B
y_c^{OPT}	0.0448	0.0576	0.0450	0.0569	0.058	0.074
y_c^{MFA}	0.0630	0.081	0.0630	0.081	0.0630	0.081
ξ/a	7.143	5.555	7.143	5.555	7.143	5.555

$$\lim_{x\to 0} kTI_3(\eta,\mu,T) = \mathrm{sgn}(\mu)\theta(\mu-\eta)\sqrt{\mu^2-\eta^2}. \quad (6.3)$$

Using Eqs. (6.1)–(6.3) in Landau's free energy density, Eq. (3.5), we notice that it can be divided into two cases: (i) $\mu<\eta$ and (ii) $\mu>\eta$. At zero temperature, the critical chemical potential $\mu_c(0)$ is defined as the one which produces the same pressure for both $\bar{\Delta}_c=\Delta_0\neq 0$ and $\bar{\Delta}_c=0$. This quantity, which was evaluated in Ref. 21, is given by

$$\mu_c(0) = \frac{M}{\sqrt{2}}\exp\left\{-\frac{\pi}{\lambda_{\mathrm{GN}}\left(1-\frac{1}{2N}\right)}\right\}\left(1-\frac{\lambda_{\mathrm{GN}}}{2\pi N}\right)^{-1/2}. \quad (6.4)$$

As expected, there are two values of ρ corresponding to $\mu_c(0)$. The first is simply $\rho=0$, which corresponds to the minimum of the free energy density that occurs at $\bar{\Delta}_c=\Delta_0\neq 0$ for the case $\mu<\eta$ (corresponding to the $T=\mu=0$ situation). In the second case ($\mu>\eta$), the minimum of the free energy density occurs at the origin $\bar{\Delta}_c=0$. In this case, the PMS relation, Eq. (3.9), implies that $\bar{\eta}=0$ and one gets, from Eq. (3.11) and after simple algebra, the result

$$\rho_c(0) = \frac{\mu_c(0)N}{\pi\hbar v_F}\left(1-\frac{\lambda_{\mathrm{GN}}}{2\pi N}\right), \quad (6.5)$$

where the multiplicative factor in the RHS of the above equation, $\mu_c(0)N/(\pi\hbar v_F)$, is just the MFA result (with $N=2$). In Eq. (6.5), the term $\lambda_{\mathrm{GN}}/(2\pi N)$ gives the first order OPT finite N corrections to $\rho_c(0)$. One can now insert Eq. (6.4) into Eq. (6.5). Using also the expression for Δ_0, Eq. (4.1), we obtain an analytical expression for the critical density that includes finite N corrections:

$$y_c(0) = a\rho_c(0) = \frac{\sqrt{2}N\Delta_0}{\pi W}\left(1-\frac{\lambda_{\mathrm{GN}}}{2\pi N}\right)^{1/2}\left(1-\frac{1}{2N}\right), \quad (6.6)$$

where we have used the defining relation $a/(\hbar v_F)=2/W$. Note that the explicit (overall) scale M dependence disappears from Eq. (6.6), where only the physical parameters W/Δ_0 set the overall scale. However, there is an implicit scale dependence in the OPT case via the dependence on $\lambda_{\mathrm{GN}}(M)$ within the factor $[1-\lambda_{\mathrm{GN}}/(2\pi N)]^{1/2}$. Note, however, that since $[1-\lambda_{\mathrm{GN}}/(2\pi N)]^{1/2}\to 1$ as $N\to\infty$, the MFA results only depend on the ratio $\Delta_0/W=E_{\mathrm{gap}}/W=a/\xi$.

Concerning our third prescription, the "effective mean field" (EMF) prescription III defined in Sec. IV, wherein the OPT corrections are differently reinterpreted as redefining effective coupling and scale, the derivation of the corresponding expression of the critical dopant concentration is straightforward if using the definition in Eq. (4.5) and reads

$$y_c^{EMF}(0) = \frac{\sqrt{2}N\Delta_0}{\pi W^*_{EMF}}\left[1-\frac{\lambda^*_{EMF}}{2\pi N\left(1-\frac{1}{2N}\right)}\right]^{1/2}, \quad (6.7)$$

where it is again understood that corresponding set A or B data values should be used now for λ^*_{EMF} and W^*_{EMF}.

We are now in a position to make predictions concerning the observable $y_c(0)$ by using, for completeness, the two different sets of data parameters and our three different theoretical prescriptions. The comparison between the OPT and MFA results is shown in Table II.

As one can see from Table II, the results depend rather substantially on the experimental data set choice, essentially due to the (linear) dependence on Δ_0. The most quoted experimental value of y_c is $y_c\sim 0.06$, although its precise value is not very accurately determined. Typically, looking, e.g., at the data from Refs. 7 and 39, one may infer non-negligible uncertainties on the exact transition value of about $\Delta y_c\sim 0.01$. Also, slightly higher values of y_c have been reported in other studies.[40] In contrast, the two different prescriptions I and II regarding the scale dependence only mildly affect the y_c values in the OPT case, i.e., the arbitrary scale dependence, which only indirectly appears within the factor $[1-\lambda_{\mathrm{GN}}/(2\pi N)]$, which appears in our previous expressions such as Eq. (6.6), remains moderate.

Inspection of Table II indicates that the OPT performs better for smaller values of ξ/a. We have carried out numerical simulations that indicate that, in fact, the OPT and MFA predict similar deviations from the experimental value, $y_c=0.06$, for $\xi/a\simeq 6.4$. For $\xi/a<6.4$, however, the OPT predictions are better than the MFA ones and the situation gets reversed for $\xi/a>6.4$ as Table II shows. To illustrate this point, we present Fig. 3, where $y_c(0)$ is plotted as a function of ξ/a, using prescription IB (Table I). This figure shows that for the value $\xi/a=6$, which Ref. 19 refers to, the OPT ($y_c=0.0535$) performs better than the MFA ($y_c=0.0750$). We also remark that the same pattern is obtained when one considers other sets of values and prescriptions.

Finally, as far as the different prescriptions are concerned, we note that the ones that make use of the band gap energy as 1.8eV (used in our data sets B in Table I), produces results with much better agreement with the experimental data for the OPT than the MFA, as one can check from the results in

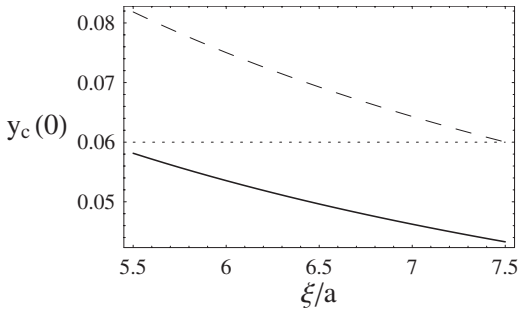

FIG. 3. The OPT (continuous line) and MFA (dashed line) predictions for $y_c(0)$ as a function of ξ/a, using prescription IB (Table I), in the relevant range $5.5 \leq \xi/a \leq 7.5$. The experimental value is $y_c(0) \simeq 0.06$.

Table II. In fact, this value for the band gap energy appears in the literature as a more satisfactory value for polyacetylene.[6]

B. Finite temperature case

To obtain the temperature dependence of the critical dopant concentration, one can numerically proceed by considering $y_c(T)=a\rho_c(T)$. First, as already emphasized, one should note that in practice, there is an upper temperature of about $T_d \sim 400$K, above which our simple models break down since the polymer undergoes other phase transitions. Figure 4 shows that from the absolute zero temperature to the upper temperature, our prediction to the decrease in the critical dopant concentration is only about 1%, while it is less than 0.5% from room temperature (about 300 K), at which most of the experiments are done, to the upper temperature. This shows that in practice, at least with the type of models considered here, one may safely evaluate y_c at $T=0$ as it has been done in Refs. 17 and 18.

VII. CONCLUSIONS

By using the OPT, we have reviewed the evaluation of Landau's free energy for the 1+1 dimensional massless Gross–Neveu model at finite temperature and chemical potential as performed in Ref. 21. Then, relating this model to the TLM continuous model for polyacetylene, we have computed the critical dopant concentration y_c for the transition to the metallic phase. The (divergent) free energy density has been rendered finite by using a renormalization procedure that is standard in quantum field theories ($\overline{\text{MS}}$ scheme with dimensional regularization). An arbitrary energy scale M, which was introduced during the formal regularization process, was fixed by using polyacetylene experimental inputs. Regarding the matching of the theory parameters to the experimental data values, we have provided a critical discussion of the possible different prescriptions to relate them giving, at the same time, the expected results for each of the prescriptions used.

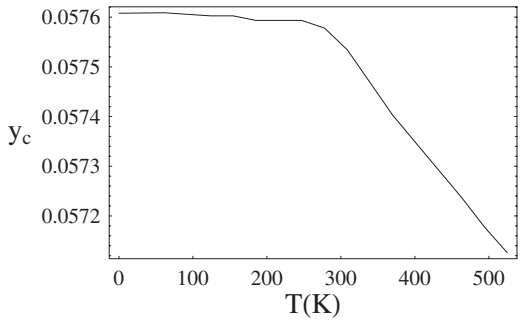

FIG. 4. The critical dopant concentration, $y_c(T)$, vs temperature dependence for parameter set B and procedure I. The degradation temperature is about $T \approx 400$K.

The OPT formalism allows for the inclusion of finite N corrections already at the first nontrivial order, which should improve the usual MFA results since, for this particular case, $N=2$. To illustrate the possible phase transitions allowed by the GN model, we have obtained phase diagrams in the $T-\mu$, as well as in the $T-\rho$ planes. Then, we have obtained a neat analytical expression for $y_c=a\rho_c$ at $T=0$ which contains explicit $1/N$ corrections. Our results show that when one uses up-to-date parameter values, the OPT results improve over the MFA as expected and are in good agreement with the experimental result. Another result of the present work regards the study of possible thermal effects in y_c. Our analysis has been performed in a numerical fashion, which shows that for a realistic temperature range $0<T<400$K, thermal effects induce a negligible decrease of y_c when going from the (mixed) semiconducting phase to the (symmetric) metallic phase.

Regarding the metal-insulator transition, one must recall the importance of the transport property and the localization problem.[41,42] As far as polymers are concerned, it is known that their transport properties result from the mechanism of hopping,[42] which leads the conductivity to increase with the temperature until some maximum value. At the same time, the disorder in the system can result in the localization of states, and if it is too strong, it can lead to an insulator behavior. The metal-insulator transition in real systems is then a consequence of the interplay of the amount of disorder, doping, and the thermal activation processes. On the theoretical side, an interesting possibility of extending the field theory application method we used to study the metal-insulator transition in polyacetylene would be the calculation of the conductivity σ and the determination of its T,μ dependence. This would then allow a closer comparison to the experimental measures on this quantity. Basically, from response theory, the conductivity can be computed from a Green–Kubo formula, which entails a calculation of specific correlation functions and higher loop Feynman diagram contributions in the GN model we used. Although the calculation of σ in this context has been already considered within other approaches and approximations in the literature, we hope to pursue a detailed calculation of $\sigma(T,\mu,N)$, including finite N corrections, which we believe has not been done up to now. However, this is a nontrivial calculation that is well beyond the scope of the present paper. We intend to address this issue in the future. Another interesting possible extension of the present work would be to use the OPT and the methods developed in Ref. 34 to consider the massive GN model, which can be related to *cis*-polyacetylene.

ACKNOWLEDGMENTS

H.C., M.B.P., and R.O.R. were partially supported by CNPq-Brazil. H.C. thanks FAPEMIG for partial support. The authors are grateful to A. Heeger for a private communication regarding the experimental values of polyacetylene. The authors thank V. Mano for helpful information on thermal properties of polyacetylene and M. Thies for sending us an important reference.

*hcaldas@ufsj.edu.br
†kneur@lpta.univ-montp2.fr
‡marcus@fsc.ufsc.br
§rudnei@uerj.br

[1] H. Shirakawa, E. J. Louis, A. G. MacDiarmid, C. K. Chiang, and A. J. Heeger, J. Chem. Soc., Chem. Commun., 578 (1977).
[2] J. H. Burroughes, C. A. Jones, and R. H. Friend, Nature (London) **335**, 137 (1988).
[3] Y. Yu, M. Nakano, and T. Ikeda, Nature (London) **425**, 145 (2003).
[4] S. Kubatkin, A. Danilov, M. Hjort, J. Cornil, J.-L. Bredas, N. Stuhr-Hansen, P. Hedega, and T. Bjørnholm, Nature (London) **425**, 698 (2003).
[5] X. Lin, J. Li, and S. Yip, Phys. Rev. Lett. **95**, 198303 (2005).
[6] A. J. Heeger, S. Kivelson, J. R. Schrieffer, and W. P. Su, Rev. Mod. Phys. **60**, 781 (1988).
[7] J. Chen, T.-C. Chung, F. Moraes, and A. J. Heegerr, Solid State Commun. **53**, 757 (1985); F. Moraes, J. Chen, T.-C. Chung, and A. J. Heeger, Synth. Met. **11**, 271 (1985).
[8] W. P. Su, J. R. Schrieffer, and A. J. Heeger, Phys. Rev. Lett. **42**, 1698 (1979); Phys. Rev. B **22**, 2099 (1980).
[9] See, for example, X. Lin, J. Li, C. J. Forst, and S. Yip, Proc. Natl. Acad. Sci. U.S.A. **103**, 8943 (2006).
[10] H. Takayama, Y. R. Lin-Liu, and K. Maki, Phys. Rev. B **21**, 2388 (1980).
[11] M. V. Mostovoy and J. Knoester, Phys. Rev. B **53**, 12057 (1996).
[12] S. A. Brazoviskii and N. N. Kirove, JETP Lett. **33**, 4 (1981); Pis'ma Zh. Eksp. Teor. Fiz. **33**, 6 (1981); D. K. Campbell and A. R. Bishop, Phys. Rev. B **24**, 4859 (1981); Nucl. Phys. B **200**, 297 (1982); V. A. Osipov and V. K. Fedyanin, Theor. Math. Phys. **73**, 1296 (1987).
[13] D. Gross and A. Neveu, Phys. Rev. D **10**, 3235 (1974).
[14] U. Wolff, Phys. Lett. B **157**, 303 (1985).
[15] E. Fradkin and J. E. Hirsch, Phys. Rev. B **27**, 1680 (1983).
[16] A. Saxena and A. R. Bishop, Phys. Rev. A **44**, R2251 (1991).
[17] A. Chodos and H. Minakata, Phys. Lett. A **191**, 39 (1994).
[18] A. Chodos and H. Minakata, Nucl. Phys. B **490**, 687 (1997).
[19] D. K. Campbell, Synth. Met. **125**, 117 (2002).
[20] A. Okopinska, Phys. Rev. D **35**, 1835 (1987); A. Duncan and M. Moshe, Phys. Lett. B **215**, 352 (1988).
[21] J.-L. Kneur, M. B. Pinto, and R. O. Ramos, Phys. Rev. D **74**, 125020 (2006); Braz. J. Phys. **37**, 258 (2007).
[22] E. C. Marino and L. H. C. M. Nunes, Nucl. Phys. B **741**, 404 (2006), and references therein.
[23] J.-L. Kneur, M. B. Pinto, R. O. Ramos, and E. Staudt, Phys. Rev. D **76**, 045020 (2007).
[24] K. G. Klimenko, Z. Phys. C **37**, 457 (1988); B. Rosenstein, S. H. Park, and B. J. Warr, Phys. Rev. D **39**, 3088 (1989); B. Rosenstein, B. J. Warr, and S. H. Park, Phys. Rev. Lett. **62**, 1433 (1989).
[25] J.-L. Kneur, M. B. Pinto, R. O. Ramos, and E. Staudt, Phys. Lett. B **657**, 136 (2007).
[26] F. F. de Souza Cruz, M. B. Pinto, and R. O. Ramos, Phys. Rev. B **64**, 014515 (2001); Laser Phys. **12**, 203 (2002).
[27] J.-L. Kneur, A. Neveu, and M. B. Pinto, Phys. Rev. A **69**, 053624 (2004); J.-L. Kneur and M. B. Pinto, *ibid.* **71**, 033613 (2005); B. Kastening, *ibid.* **70**, 043621 (2004).
[28] J.-L. Kneur, M. B. Pinto, and R. O. Ramos, Phys. Rev. Lett. **89**, 210403 (2002); Phys. Rev. A **68**, 043615 (2003).
[29] E. Braaten and E. Radescu, Phys. Rev. Lett. **89**, 271602 (2002); Phys. Rev. A **66**, 063601 (2002).
[30] L. D. Landau and E. M. Lifshtiz, *Statistical Physics* (Pergamon, New York, 1958), p. 482.
[31] N. D. Mermin and H. Wagner, Phys. Rev. Lett. **17**, 1133 (1966).
[32] S. Coleman, Commun. Math. Phys. **31**, 259 (1973).
[33] R. F. Dashen, S.-K. Ma, and R. Rajaraman, Phys. Rev. D **11**, 1499 (1975); S. H. Park, B. Rosenstein, and B. Warr, Phys. Rep. **205**, 108 (1991).
[34] O. Schnetz, M. Thies, and K. Urlichs, Ann. Phys. (N.Y.) **314**, 425 (2004); M. Thies and K. Urlichs, Phys. Rev. D **72**, 105008 (2005); M. Thies, J. Phys. A **39**, 12707 (2006).
[35] P. M. Stevenson, Phys. Rev. D **23**, 2916 (1981); Nucl. Phys. B **203**, 472 (1982).
[36] S. K. Gandhi, H. F. Jones, and M. B. Pinto, Nucl. Phys. B **359**, 429 (1991).
[37] T. Anderson and S. Roth, Braz. J. Phys. **24**, 746 (1994).
[38] L. W. Shacklette and J. E. Toth, Phys. Rev. B **32**, 5892 (1985).
[39] T. C. Chung, F. Moraes, J. D. Flood, and A. J. Heeger, Phys. Rev. B **29**, 2341 (1984).
[40] E. M. Conwell, H. A. Mizes, and S. Jeyadev, Phys. Rev. B **40**, 1630 (1989).
[41] A. B. Kaiser, Rep. Prog. Phys. **64**, 1 (2001).
[42] V. N. Prigodin and A. J. Epstein, Synth. Met. **125**, 43 (2002).